The dolerite dyke swarm of Mongo, Guéra Massif (Chad, Central Africa): Geological setting, petrography and geochemistry

Oumarou Faarouk Nkouandou, Jacques-Marie Bardintzeff, Oumar Mahamat, Aminatou Fagny Mefire, Alembert Alexandre Ganwa

Research Article **Open Access**

Oumarou Faarouk Nkouandou, Jacques-Marie Bardintzeff*, Oumar Mahamat, Aminatou Fagny Mefire, and Alembert Alexandre Ganwa

The dolerite dyke swarm of Mongo, Guéra Massif (Chad, Central Africa): Geological setting, petrography and geochemistry

DOI 10.1515/geo-2017-0012
Received Feb 08, 2016; accepted Mar 11, 2017

Abstract: Dolerite dykes are widespread in the Mongo area within the granitic Guéra Massif (Chad, Central Africa). Dykes are several hundred metres to several kilometres long, a metre to decametre thick, and vertical, crosscutting the Pan-African granitic basement rocks. They are controlled by major Pan-African NNE-SSW, NE-SW and ENE-WSW faults. Rocks constituting the dykes exhibit typical doleritic textures (*i.e.* intergranular, ophitic or subophitic). They are mainly composed of phenocrysts, microcrysts and microlites of clinopyroxene, amphibole, plagioclase, alkali feldspar and Fe-Ti oxides. Mongo dolerites are classified into two groups: Group 1 of basalt and trachybasalt and Group 2 of basaltic trachyandesite, which follow a trend with continental tholeiite affinities, and are differentiated through fractional crystallization. Trace element enrichment and REE contents show the high melting degree at shallow depths of enriched sub-continental lithospheric mantle, whose composition is intermediate between OIB and MORB, contaminated by small amounts of sediment during older subduction. Mongo dolerites are interpreted as imprints of either the final stage of stabilization of ancient continental crust, or the initiation of tectonic activity related to Pan-African mobile belts.

Keywords: dolerite; dyke; Pan-African; Mongo; Guéra Massif; Chad

***Corresponding Author: Jacques-Marie Bardintzeff:** Univ Paris-Sud, Sciences de la Terre, Volcanologie, Planétologie, UMR CNRS 8148 GEOPS, bât. 504, Université Paris-Saclay, F-91405 Orsay, France; Email: jacques-marie.bardintzeff@u-psud.fr; Tel: (33) (1) 69 15 67 44

Oumarou Faarouk Nkouandou, Oumar Mahamat, Aminatou Fagny Mefire, Alembert Alexandre Ganwa: Faculty of Science, Department of Earth Science, University of Ngaoundéré, Ngaoundéré, Cameroon

1 Introduction

Precambrian massifs are exposed in Chad as five terranes (review in [1]): Tibesti to the north [2], Waddai to the east, Mbaibokoum, or Yade, to the south [3], Mayo Kebbi to the south-west [4–7] (Figure 1A) and Guéra to the south [8]. Mayo-Kebbi and Mbaibokoum/Yade constitute terranes of the Neoproterozoic Central African Orogenic Belt (CAOB) [4, 5]. Tibesti, Waddaï and Guera are parts of a large area coined by [9] as the "Saharan Metacraton", defined as “a craton that has been remobilized during an orogenic event but that is still recognizable dominantly through its rheological, geochronological and isotopic characteristics” [9]. This paper presents petrology and geochemistry data on the doleritic dyke swarms of Mongo and discusses their relevance to tectonic reconstitution of the Guéra Massif.

2 Geological setting

Doleritic dykes are widespread in the Mongo area within the granitic Guéra Massif (Chad, Central Africa). These dykes occur in Oyo, Zobili and Ibine massifs, and close to Barlo and Tialo Ideba villages (Figure 1).

Previous studies carried out in Guéra Massif mainly concern mineral prospecting and exploration, and mineral deposit investigations particularly before 1960 [see 1].

The most recent work on the Guéra Massif basement offers new evidence from field observations and remote sensing studies [8]. Four groups of rocks have been distinguished, based on relative chronology: (1) gabbroic rocks, (2) diorites, granodiorites, and hornblende-biotite granites, (3) two-mica granites and (4) biotite granites [8]. From a structural point of view, the D1 and D2 deformation phases have affected the Mongo doleritic dyke swarm, but are lacking in two-mica granites and biotite granites. The third deformation phase D3 is associated with N25-75°E

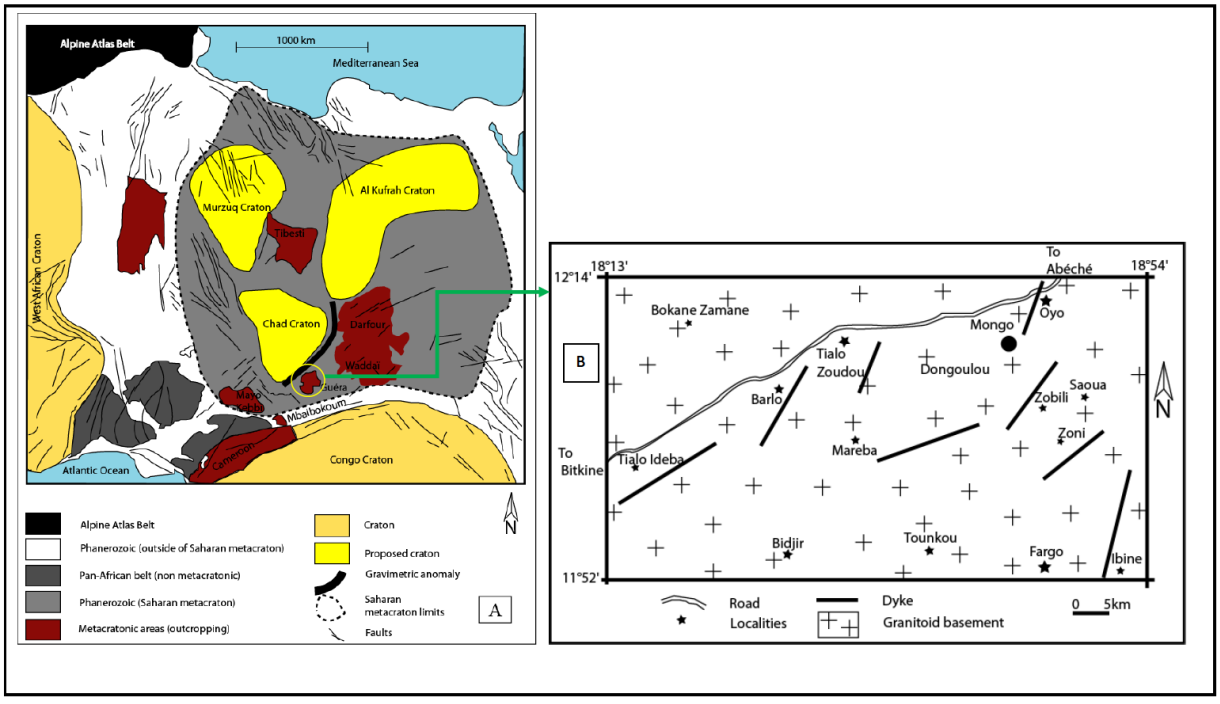

Figure 1: A: Main domains of Saharan Africa centred on the Saharan metacraton (modified from [51]) and B: Geological map of Mongo area, showing dykes and granitoid basement.

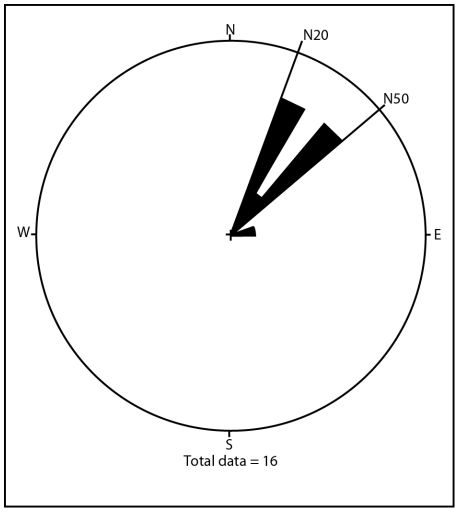

Figure 2: Rose diagram of Mongo doleritic dykes.

striking shear zones. The last deformation phase D4 is ubiquitous and responsible of brittle structures (faults and joints), oriented NE-SW and NW-SE and controlled dyke emplacement.

Dykes may be considered as issued from either late stages of the Pan-African orogeny or Phanerozoic tectonic events.

3 Materials and methods

Over 10 giant dykes are exposed in the Mongo region (Fig. 1 and 3). Each dyke was systematically sampled and its strike, dip, width and exact position (GPS) were recorded.

Petrographic studies were carried out using 14 thin sections prepared from representative samples at the GEOPS Laboratory, University Paris-Sud Orsay-CNRS, France. Major and trace element analyses of lavas were determined using 8 representative samples by ICP-AES and ICP-MS at the Acmel Laboratory of Vancouver, Canada. Prepared samples were mixed with $LiBO_2/Li_2B_4O$ flux. Crucibles were fused in a furnace. The cooled beads were dissolved in ACS-grade nitric acid and analyzed by ICP and/or ICP-MS.

4 Results

4.1 Fieldwork and petrography

The granitoid basement of the Mongo area is dissected by numerous vertical and sub-vertical mafic dykes striking mainly N20-N30, NE-SW and occasionally N70-80 (Figure 2). They remain typically parallel to the principal stress

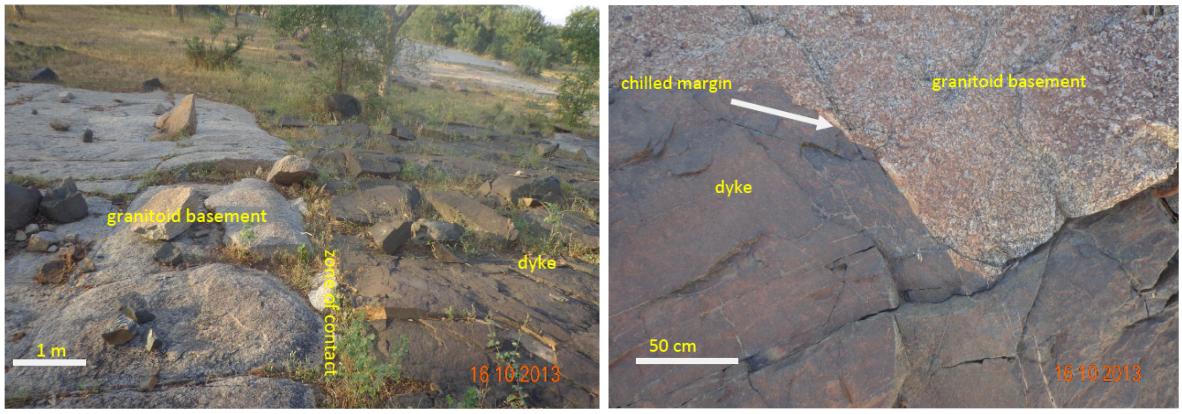

(a) (b)

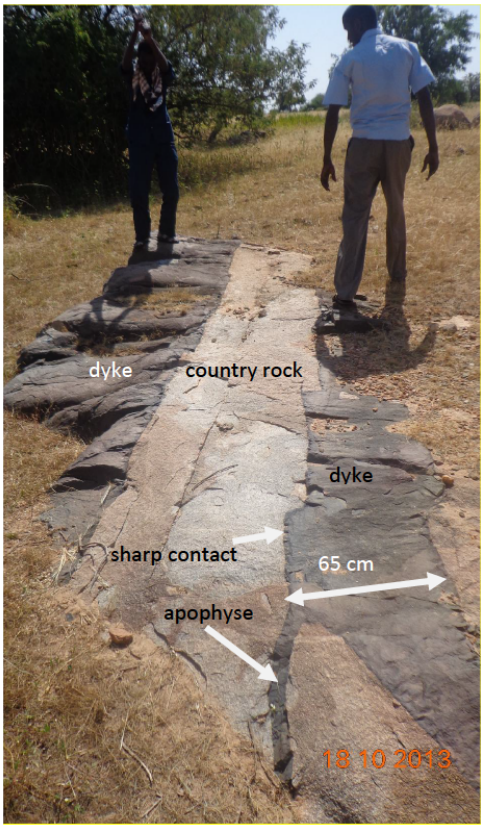

(c)

Figure 3: A: Sharp contact between granitoid wall-rock and Kilim dyke, B: Sharp contact between granitoid wall-rock and Kilim dyke showing a chilled margin. Increasing grain-size is obvious towards the dyke interior, C: Dyke edges with sharp contact between wall-rock and Barlo dyke.

directions, recognized by [8], that affect the Mongo basement rock. Dyke thicknesseses vary from 1.1 to 15 m at Oyo, Zobili and Barlo, and from 15 to 30 m at Ibine, with a maximum of 50-100 m at Zoni. Their lengths are usually several kilometres (Figure 1B). Contacts with wall rocks are usually sharp (Figure 3A) and display chilled margins, especially Barlo dykes, whose widths are less than 3 m (Figure 3B). Increasing grain-size toward the dyke interior is typical of the Kilim dolerite. Finger-like structures (Figure 3C) developed sometimes at the edges. Such features indicate that Mongo dykes were emplaced along pre-existing fractures.

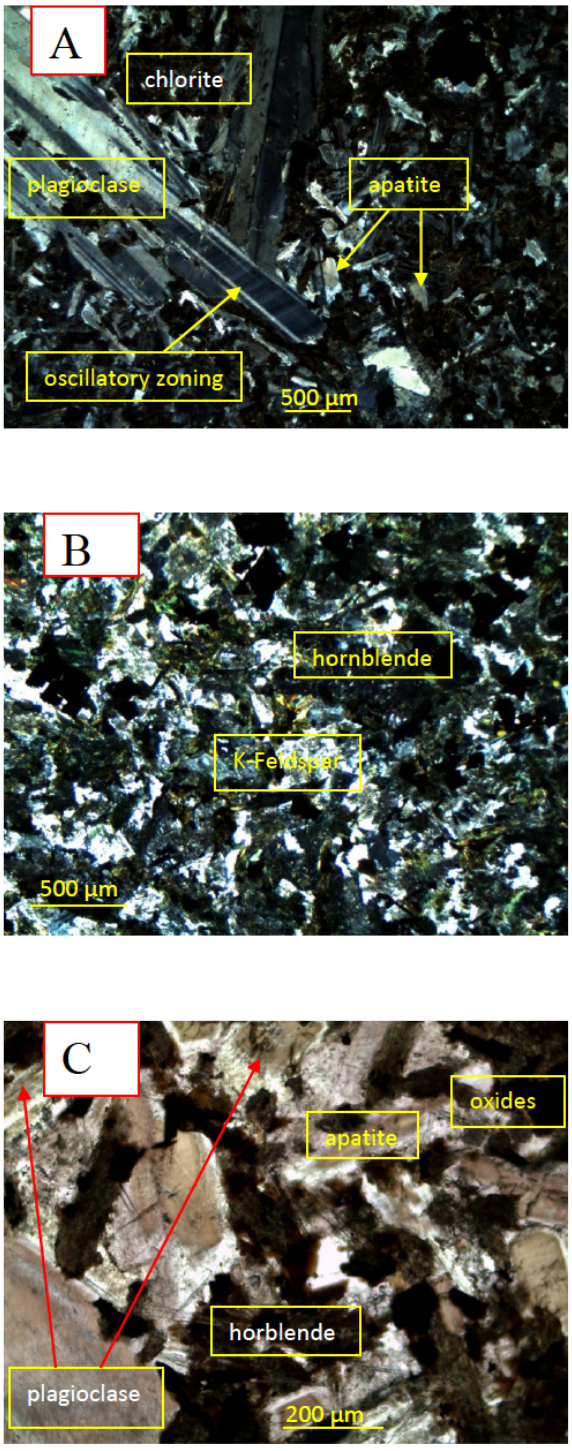

Figure 4: Cross-polarized light photomicrographs of the main representative samples. A: Skeletal plagioclase phenocrysts with oscillatory zoning and wispy feldspar lamellae in subdoleritic texture of Mongo dyke (MZO1). B: Secondary minerals of chlorite composition and alkali-feldspar in Kilim dyke (MZ1). C: Doleritic texture with plagioclase, apatite, feldspar and Fe-Ti oxides phenocrysts with clinopyroxene oikocryst (MK2).

Oyo and Zoni dykes are strongly weathered and form both an arena of blocks and 50 cm to several metre-size bowls. Dykes may be affected by secondary alteration, or contain epidote streaks along cracks. Yet, fresh outcrops are available for sampling. Representative samples are medium- to coarse-grained and dark-grey to dark-green in colour. Whitish feldspar crystals with tabular shape (1 × 3 mm to 3 × 7 mm, up to 30% in volume) are easily observed within the dark matrix. Blocky pyroxene crystals (7 to 20% in volume) are darker than the matrix. Glittering acicular pyroxene crystals (< 5% in volume) are present in some samples.

Under plain polarized light (Figure 4A, 4B and 4C), dykes exhibit subdoleritic and seriate texture. They are composed of plagioclase phenocrysts exhibiting swallow-tail terminations and skeletal features, sometimes decorated with a zone of small inclusions and surrounded by wispy feldspar lamellae (Figure 4A). Phenocrysts and microphenocrysts of alkali feldspar occur also in some samples. Clinopyroxene oikocrysts, apatite, scarce skeletal green amphibole and Fe-Ti oxides are present.

4.2 Geochemistry

Major element data of fresh representative samples are listed in Table 1. Mongo dolerites display various chemical compositions. Two groups may be distinguished: Group 1 is SiO_2-poor (48.3-51.2 wt%) but Ti-rich (2.5-3.7 wt% TiO_2), whereas Group 2 is SiO_2-richer (52.1-55.1 wt%) but TiO_2-poorer (1.8-2.7 wt%). Group 1 is alkali poorer: K_2O contents are 1.5-1.9 and 2.5-3.3 wt%, respectively for Group 1 and Group 2, and Na_2O contents are 3.0-3.3 and 3.6-3.7 wt%. Al_2O_3 (13.9-15.3 and 14.1-15.8 wt%, respectively for Group 1 and Group 2), P_2O_5 (0.7-1.1 and 0.5-1.4 wt%) and Fe_2O_3 (13.1-16.5 and 11.5-13.6 wt%) contents are relatively similar in the two groups. There is a positive correlation between TiO_2 and P_2O_5 (not shown in the accompanying figures). MgO contents (2.6-5.1 wt%), and corresponding Mg# (= 100*MgO/40.32 / ((MgO/40.32) + (Fe_2O_3/71.85)) ratios between 27.8 and 40.3, are low. In the (Na_2O+K_2O) vs SiO_2 diagram, Group 1 is composed of basalts and trachybasalts, whereas Group 2 is composed of basaltic trachyandesites (Figure 5).

Contents of transition elements (Ni: less than 20 up to 45 ppm, Co: 17-39 ppm, V: 133-212 ppm and Cu: 13-35 ppm) are low compared with typical primitive mantle magma values, e.g., Ni (250-350 ppm) and Co (50-70 ppm) [10, 11]. Doleritic liquids could have derived from a source depleted in these elements and/or early fractionation of

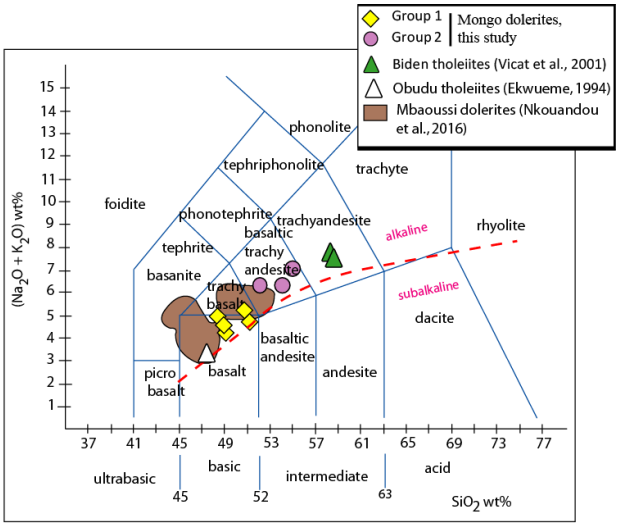

Figure 5: Mongo dolerite compositions plotted in the TAS diagram (after [52]). Dashed curve separates alkaline from subalkaline fields (from Miyashiro [22]).

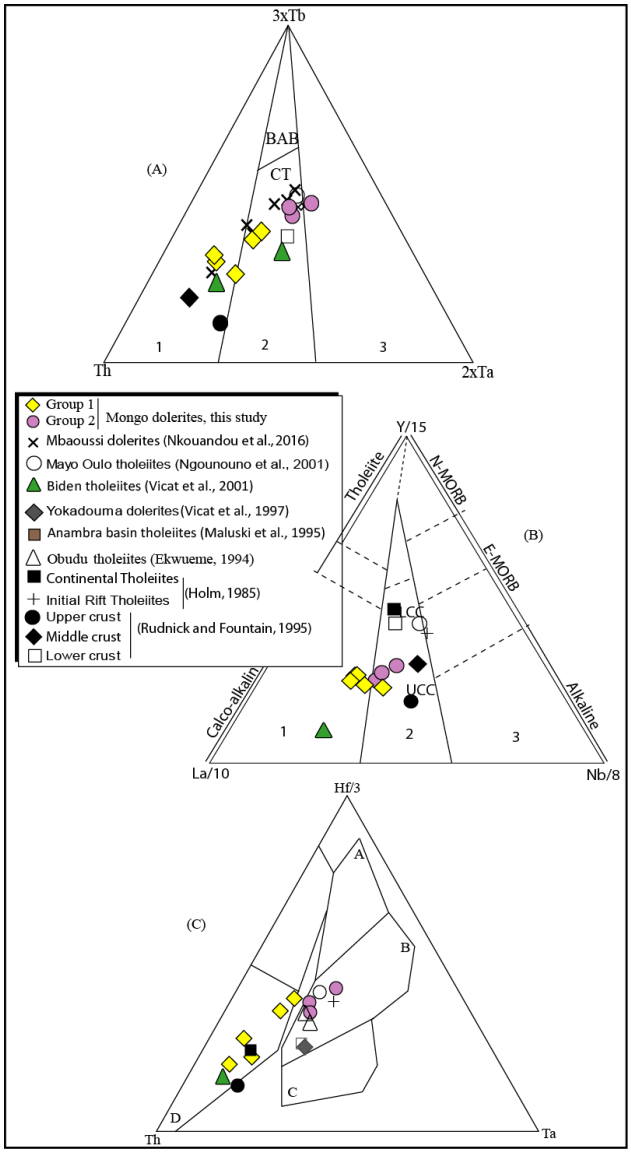

Figure 6: Mongo dolerite Group 1 and Group 2 in triangular diagrams. (A): Th-Tb-Ta [17], 1: Orogenic basalts, 2: Continental tholeiites and arc basin basalts, 3: Non orogenic basalts, BAB: Back Arc Basin Basalt, CT: Continental Tholeiites, (B): La-Y-Nb [20], 1: Arc-related orogenic series, 2: Intermediate domain of continental tholeiites, 3: Anorogenic series of oceanic ridges and intraplate alkaline basalts, CC: Continental Crust (mean value), UCC: Upper Continental Crust, (C): Th-Hf-Ta [45], A: N-type MORB, B: E-type MORB and tholeiitic within-plate basalts and differentiates, C: Alkaline within-plate basalts and differentiates, D: Destructive plate-margin basalts and differentiates.

Mg-olivine, clinopyroxene and Fe-Ti oxides that occurred in the parental magma.

Alkali-earth element Sr (430-700 ppm) and Ba (800-1300 ppm) contents are high and close to those of Biden dolerites in the Adamawa plateau, Cameroon [12] which exhibit very high Ba contents (up to 1802 ppm). Rb contents (28-76 ppm) show a wide range and are higher than in Mayo Oulo-Léré dolerites, Cameroon (10 ppm, [13]) and the Neoproterozoic flood basalts (≈ 4 ppm) of the lower Dja, Yokadouma and Nola, Cameroon [14]. HFSE contents (Ta, Nb, Hf, Th, Y and, to a lesser degree, Zr) are high and decrease from the primitive of Group 1 to the slightly evolved samples of Group 2. Conversely, U and Th contents increase from Group 1 to Group 2, whereas Hf shows overlapping content values.

Y/Nb ratios are always > 1 and vary between 1.35 and 2.2 with the highest values found in evolved samples. Zr/Nb ratios in Group 1 (12.3-13.8) are nearly constant, whereas they are fairly higher in Group 2 (11-21). Ratios in both groups are similar to E-MORB (between 10 and 20, [15]). Nb/Ta ratios (15-18 for Group 1 and 14-21 for Group 2), as well as Zr/Hf ratios (41-42.5 for Group 1 and 39-47 for Group 2) recall marine sediments or upper continental crust values (Nb/Ta: 14.2±1.8 and Zr/Hf: 35, [16]). Th/Ta ratios increase from Group 1 (1.3-2.0) to Group 2 (2.7-8.0). Th/Nb ratios are nearly constant (≈ 0.1) in Group 1 and vary from 0.2 to 0.4 in Group 2 dolerites. In the Th-Tb-Ta diagram (Figure 6A, after [17]), Mongo dolerites display an array of continuous variation from Group 1 to Group 2, especially within the field of continental tholeiite or contaminated magmas. High Ba/Nb (31-74), Ba/La (20-30), Rb/Nb (1.1-4.2), K/Nb (562-1572), La/Nb (1.5-3.0) ratios vary in the same range with systematic increase from Group 1 to Group 2, excepting Ce/Pb (14-40) ratios which are decreasing. Nb/U ratios show contrasting values, between 22 and 52 in Group 1 and 11-18 in Group 2.

Table 1: Major and trace element compositions of Mongo dolerites. LOI-free total recalculated at 100.00. CIPW normative compositions calculated assuming Fe_2O_3/FeO ratio of 0.15.

Location	11°27'03"N 18°27'26"E	11°25'79"N 18°25'09"E	11°27'43"N 18°27'03"E	12°20'18"N 18°12'44"E	12°19'12"N 18°13'01"E	12°08'37"N 18°16'01"E	11°27'43"N 18°26'6"E	12°07'17"N 18°16'04"E
Sample	MZO1	MK2	MK3	MO3	MO4	MZ1	MT2	MZ2
SiO_2 (wt%)	48.35	48.93	48.88	50.75	51.17	52.13	54.22	55.09
TiO_2	3.71	3.09	3.05	2.47	2.73	2.66	1.78	2.12
Cr_2O_3	0.01	0.01	0.01	0.01	0.02	0.00	0.00	0.00
Al_2O_3	13.89	15.07	15.24	15.22	14.95	14.08	15.83	15.13
Fe_2O_3	16.47	14.32	14.46	13.52	13.12	13.61	11.48	12.05
MnO	0.20	0.18	0.20	0.18	0.17	0.18	0.15	0.18
MgO	4.16	5.06	5.06	4.85	4.98	3.38	3.91	2.60
CaO	7.16	7.83	7.64	7.07	7.19	6.30	5.88	5.25
Na_2O	3.17	3.01	3.01	3.25	2.98	3.56	3.72	3.66
K_2O	1.75	1.50	1.64	1.94	1.70	2.69	2.54	3.32
P_2O_5	1.13	1.00	0.81	0.74	0.98	1.41	0.49	0.60
Sum	100.00	100.00	100.00	100.00	100.00	100.00	100.00	100.00
CIPW norm								
Quartz	0.00	0.00	0.00	0.00	2.51	1.56	1.41	3.14
Corundum	0.00	0.00	0.00	0.00	0.00	0.00	0.00	0.00
Orthoclase	10.16	8.81	9.72	11.46	9.99	15.84	14.71	19.56
Albite	26.40	25.30	25.45	27.50	25.05	30.04	30.80	30.89
Anorthite	18.24	23.00	23.22	21.21	22.21	14.43	18.63	14.96
Leucite	0.00	0.00	0.00	0.00	0.00	0.00	0.00	0.00
Nepheline	0.00	0.00	0.00	0.00	0.00	0.00	0.00	0.00
Diopside	7.98	7.56	7.83	7.52	5.71	6.39	5.69	5.99
Wollastonite	0.00	0.00	0.00	0.00	0.00	0.00	0.00	0.00
Hypersthene	20.23	21.28	18.63	20.65	22.99	19.54	19.36	16.57
Olivine	1.73	1.50	3.73	1.69	0.00	0.00	0.00	0.00
Magnetite	2.80	2.45	2.49	2.33	2.24	2.34	1.94	2.07
Ilmenite	6.93	5.83	5.79	4.69	5.15	5.03	3.30	4.01
Haematite	0.00	0.00	0.00	0.00	0.00	0.00	0.00	0.00
Apatite	2.57	2.29	1.87	1.71	2.25	3.24	1.11	1.39
Mg#	31.06	38.62	38.39	39.00	40.34	30.69	37.78	27.76
Be (ppm)	<1	<1	<1	3	3	<1	3	2

Continued on next page

Table 1: ... continued

Location	11°27'03"N 18°27'26"E	11°25'79"N 18°25'09"E	11°27'43"N 18°27'03"E	12°20'18"N 18°12'44"E	12°19'12"N 18°13'01"E	12°08'37"N 18°16'01"E	11°27'43"N 18°26'6"E	12°07'17"N 18°16'04"E
Rb	34.7	27.7	29.0	46.8	38.2	69.5	71.9	76.0
Sr	636.5	693.5	571.7	593.7	658.8	543.8	469.1	435.3
Cs	0.3	0.4	0.5	0.2	1.2	1.8	1.1	0.9
Ba	1125	970	817	1007	1082	1216	804	1296
V	202	212	198	177	180	174	150	133
Co	37.2	39.3	35.7	35.1	31.1	27.5	27.8	17.8
Ni	27	45	30	36	24	<20	27	<20
Cu	32.5	26.3	35.1	29.0	22.2	12.9	31.8	21.7
Sc	22	23	26	22	23	18	16	18
Y	45.6	37.1	45.0	38.8	44.7	34.5	31.1	30.7
Zr	355.7	311.4	319.5	374.4	403.6	239.3	256.3	396.9
Nb	26.2	22.5	25.9	17.8	20.9	16.5	23.0	18.8
Hf	8.5	7.6	7.8	8.9	9.5	6.1	6.9	8.5
Ta	1.8	1.5	1.4	1.2	1.3	0.9	1.4	0.9
Th	3.4	1.9	2.8	4.1	3.5	7.2	6.6	6.5
U	0.7	0.5	0.5	0.8	0.7	1.4	1.3	1.4
Pb	3.7	4.6	3.8	2.6	2.8	4.8	5.2	6.3
Ga	21.2	21.7	19.1	19.8	20.2	19.1	18.5	21.5
Sn	2	2	2	2	2	2	3	3
W	0.9	0.5	<0.5	1.1	<0.5	0.6	1.0	<0.5
La	47.1	43.9	37.6	48.5	54.6	46.5	39.6	42.3
Ce	116.3	103.0	88.3	115.4	129.2	108.1	87.1	93.6
Pr	14.90	13.60	11.26	14.08	16.25	13.45	10.43	11.59
Nd	64.6	61.4	49.8	57.3	70.6	58.7	41.0	48.0
Sm	14.06	11.63	10.87	11.07	13.47	11.77	9.33	9.80
Eu	3.89	3.43	3.01	2.88	3.38	3.83	1.90	3.04
Gd	12.64	10.89	10.25	10.39	12.20	10.68	7.61	8.48
Tb	1.79	1.47	1.60	1.49	1.67	1.42	1.13	1.20
Dy	9.61	7.66	8.48	7.40	8.60	7.00	6.08	6.43
Ho	1.80	1.43	1.70	1.52	1.50	1.26	1.17	1.22
Er	4.49	3.76	4.44	3.86	4.58	3.73	3.27	3.51
Tm	0.62	0.53	0.67	0.51	0.59	0.52	0.46	0.46
Yb	3.88	3.15	4.00	3.52	3.63	2.87	2.99	3.20

Continued on next page

Table 1: ... continued

Location	11°27'03"N 18°27'26"E	11°25'79"N 18°25'09"E	11°27'43"N 18°27'03"E	12°20'18"N 18°12'44"E	12°19'12"N 18°13'01"E	12°08'37"N 18°16'01"E	11°27'43"N 18°26'6"E	12°07'17"N 18°16'04"E
Lu	0.55	0.47	0.59	0.50	0.52	0.38	0.47	0.44
(Ce/Yb)N	7.8	8.5	5.7	8.5	9.2	9.7	7.5	7.6
(Ce/Sm)N	2.0	2.1	2.0	2.5	2.3	2.2	2.3	2.3
(La/Sm)N	2.1	2.4	2.2	2.8	2.6	2.5	2.7	2.7

Concluded

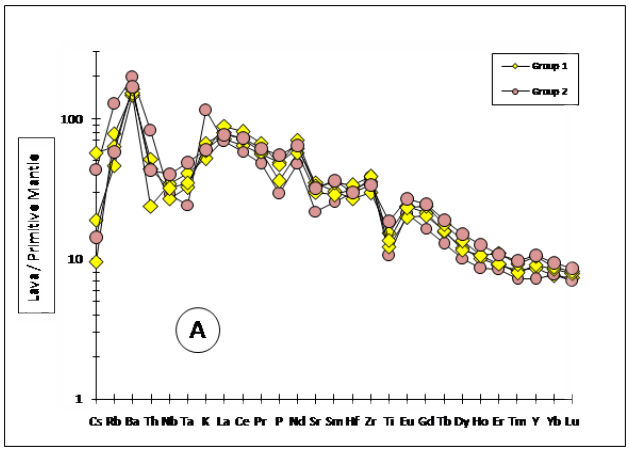

(a)

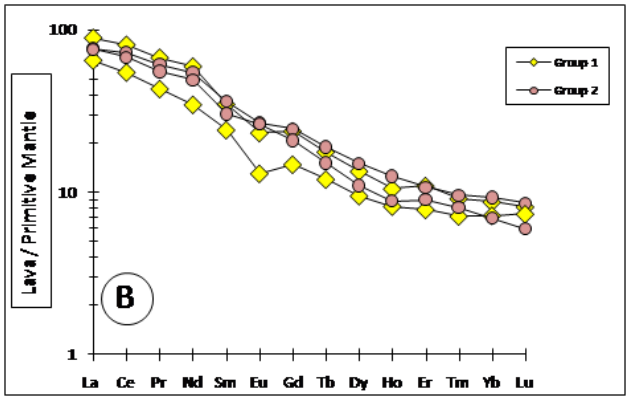

(b)

Figure 7: Primitive mantle-normalized [18] multi-element (A) and REE (B) patterns.

A primitive mantle-normalised trace-element diagram ([18], Figure 7A) exhibits fractionated patterns with increasing values from Cs to Ba and a regular decrease from Ba to Lu. The patterns are characterized by pronounced Nb, Ta, Ti and Th negative anomalies. P and, to a lesser extent, Sr negative anomalies are less pronounced. HFSE (Zr, Ti and Y) are not fractionated and Yb contents are high (> 2 ppm).

Primitive mantle-normalised REE patterns (Figure 7B) are typically LREE-rich, with distinct $(Ce/Yb)_N$ ratios (= 5.7-9.2 for Group 1 and $(Ce/Yb)_N$ = 7.5-9.7 for Group 2). The Tialo Ideba (MT1) dolerite sample yields a negative Eu anomaly (0.8<Eu/Eu*<1.0). Slight negative anomalies in Eu are noted for the other dolerites except for Zobili (MZ1). $(La/Er)_N$ and $(Gd/Er)_N$ are high and lie between 6-8 and 2.0-2.4, respectively. La/Yb ratios lie between 9-14 and 13-16 in Group 1 and Group 2, respectively.

La/Nb ratios are between 1 and 3 (Figure 8) and range between ocean basalts (MORB and OIB) and arc basalts.

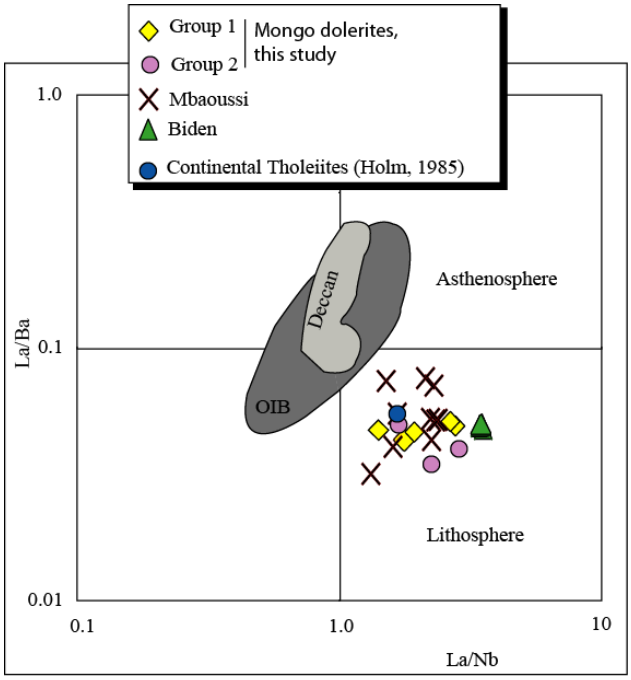

Figure 8: La/Ba vs. La/Nb ratios (after [53]) of Mongo dolerites compared with other dyke swarms.

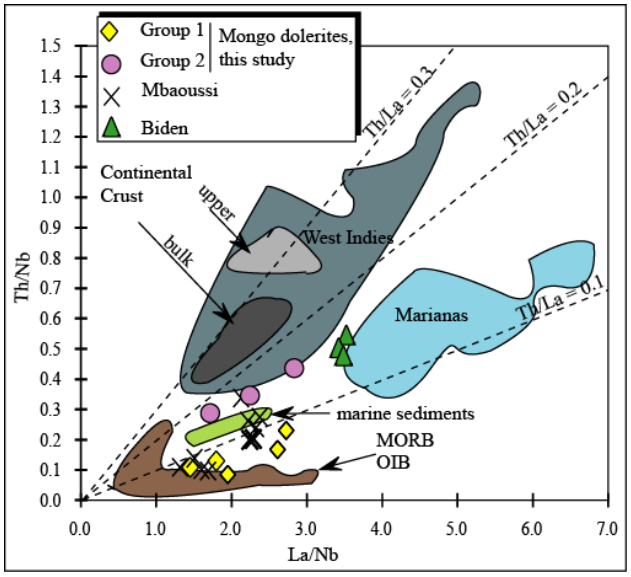

Figure 9: Th/Nb vs. La/Nb ratios. Fields from [19].

They plot near the marine sediments proposed by [19] (Figure 9). Th/La ratios in Group 1 (0.04-0.08) are typical of mantle values, whereas in Group 2 (0.15-0.17) they are typical of arc basalts and marine sediments [9]. Thus, dolerite compositions (Figure 6B) exhibit an array from active margin to late/post orogenic intra-continental fields when plotted in an La-Y-Nb diagram (after [20]).

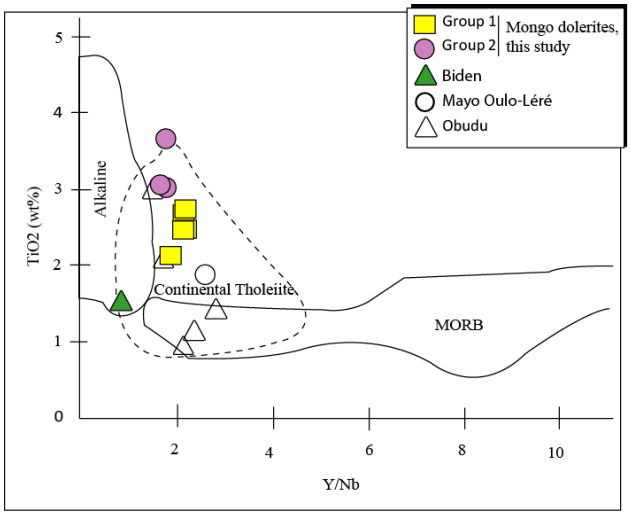

Figure 10: TiO_2 vs. Y/Nb ratios of Mongo dolerites (this study), compared with the Biden [12], Mayo Oulo-Léré [13] and Obudu [24] dyke swarms.

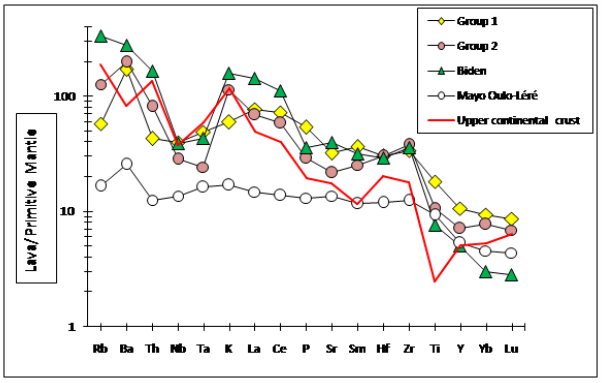

Figure 11: Primitive mantle-normalized multi-element diagrams [18] of Mongo dolerites, compared with Biden dolerites [12], Mayo Oulo-Léré dolerites related to rifting environment [13], and upper continental crust (in red, from [26]).

5 Discussion

5.1 Field evidence

The sub-vertical dykes of mafic composition from Guéra Massif trend mostly NNE-SSW, NE-SW and occasionally ENE-WSW. From field observations and remote sensing studies [8], four fracturation phases affected the Mongo basement along these same directions. Dyke emplacement was related to brittle structures, as suggested previously by [8].

Petrological and structural similarities between Mongo [8], Mayo Kebbi [4, 7] and Léré basements in Southern Chad [5] suggest that these regions are parts of the same terrane, which was welded during the Pan-African orogeny to the Adamawa-Yadé Domain [21], *i.e.* outside of the "Saharan metacraton". The NNE-SSW, NE-SW and ENE-WSW trending brittle structures could have formed between 740 and 737 Ma [4].

5.2 Mongo dolerite petrogenesis

Mongo dolerites have chemical compositions evolving from basalt to trachybasalt to basaltic trachyandesite and plot in the alkaline field of Miyashiro [22] (Figure 5). However, they share affinities with Continental Tholeiites (Figures 6 and 10) like other dolerites described in Cameroon at Biden [12] and at Likok [23] and in Nigeria at Obudu, [24]. Primitive mantle-normalized multi-element patterns of Mongo dolerites (Figure 11) are quite parallel to Biden continental tholeiites [12]. They differ clearly from Early-Cretaceous rocks of Mayo Oulo-Léré and Babouri-Figuil half-grabens in Cameroon, related to extensional structural settings [13] and from Initial Rifting Tholeiites [25]. Similarities appear between Mongo patterns and the upper continental crust pattern (after [26]), except that upper continental crust displays Ba, Sm and Ti negative anomalies.

No samples exhibit primary magma compositions. Low values of Mg# (between 27 and 40) and transition element contents (Ni<50 ppm; Co<50 ppm; V<250 ppm) differ clearly from primitive magma values [27]. Mongo dolerites differentiate by fractional crystallization, as shown by a continuous and regular decrease in MgO, CaO, P_2O_5, TiO_2 and an increase in SiO_2, Na_2O and K_2O contents from basalt to basaltic trachyandesite (Table 1). Fractionation would involve clinopyroxene, plagioclase, Fe-Ti oxides and apatite. The same fractionating assemblage can explain the continuous increase in some incompatible elements (Ba, Cs, Rb, Th and U) and decrease in Sr and Ni, Co and Sc. All samples have fractionated REE patterns, as indicated by the high $(Ce/Yb)_N$ ratios. Slight negative anomalies in Eu in REE patterns (Figure 7B) support the role played by plagioclase in the fractional crystallization process. On the other hand, the decrease of Nb, Ta, Y contents from basaltic to more evolved rocks should involve accessory mineral fractionation.

Negative anomalies in Ti, P, Sr and Cs (Figure 7A) are typical of continental tholeiite [25]. High La/Nb ratios, important variations of Zr/Nb, Zr/Hf, Nb/Ta ratios and low Nb/U ratios in Group 2 might suggest the involvement of some crustal materials or subducted sediments of continental origin in their genesis [16, 28–30]. The evolved

Group 2 rocks may have undergone contamination by the lower crust (see Figure 6A and 6B), as suggested by enrichment in K, Rb, Ba and Th and Nb negative anomalies [31]. Additional evidence is provided by a comparison of trace element patterns of Mongo dolerites with upper continental crust (Figure 11). Patterns share some similarities for the most incompatible elements but display contrasting behaviour for other elements. Sr, Nd and Pb isotopic analyses are necessary to constrain better the role played by crustal contamination. Currently, there is no field evidence to support granitoid assimilation or contamination; all contacts of the dykes with wall-rocks are sharp, with chilled margins (Figure 3B), preventing prolonged contact between the molten magma and host rocks [32]. Crustal contamination remains elusive.

5.3 Nature of the mantle source

Geochemical features indicate that Mongo dolerites derived from an enriched heterogeneous mantle source that was depleted in Nb and Ta relative to Th, U and the LREE. Magma generation would have taken place at shallow depths, aided probably by fluids generated through dehydration of old subducted slab [33]. It has been suggested [31] that continental tholeiite mantle has an intermediate composition between N and P-type MORB. Subcontinental and sub-oceanic upper mantles are compositionally distinct [34–36]. Low Th/Ta ratios of both Group 1 and Group 2 emphasize a magmatic origin [19]. On other hand, high $(La/Er)_N$ and $(Gd/Er)_N$ ratios and HREE depletion evidenced by $(Tb/Yb)_N$ between 1.7 and 2.1 suggest the presence of a garnet phase in a mantle source [37, 38].

The enrichment mechanism of Mongo dolerites' mantle source may result from an introduction of old subducted sediments into the underlying mantle as shown by Zr/Nb, Zr/Hf, Nb/Ta and Th/Ta ratios [33] and negative anomalies in Nb, Ta and Ti. The fairly high Nb/U ratio (from 22 to 52) of Group 1 is close to MORB and OIB values of 47±10 [39, 40]. Values are lower (12-18) in Group 2. Plots are intermediate between anorogenic and orogenic fields in the Th-Tb-Ta diagram (Figure 6A) [17]. Wide variations of Zr/Hf ratios could reflect compositional heterogeneity of a mantle source [41]. Thus, the best candidate for the mantle source of Mongo dolerites is the enriched sub-continental lithospheric mantle [31, 34, 43] whose composition lies between OIB and N-MORB sources (Figure 8). This source may contain a small amount of additional terrigenous subducted sediments, as illustrated in the Th/Nb vs La/Nb diagram (after [19], Figure 9) and attested by Zr/Nb ratios from 10 to 20 [37]. Th/Ta ratios from 1.6 to 4.0 [17] and high TiO_2 contents (up to 3.7 wt%), close to OIB alkali lavas [42] constitute further evidence. Mongo dolerite compositions are very distinct from typical arc-type tholeiite as proposed by Jakeš and Gill [44], shown in Th-Hf-Ta [45] and Th-Tb-Ta diagrams [17]. Accordingly, the arc-type features [46, 47] exhibited by some Mongo dolerites should be related to the addition of terrigenous sediments in mantle source, as proposed by Wayne [38] for Huronian low-Ti continental tholeiites.

5.4 Geodynamic implication

High Ba/Nb (31-74) and Th/Ta (2-5) evidence an orogenic context [46, 47], also shown in the Th-Tb-Ta diagram ([17], Figure 6A). Incompatible elements (Table 1 and Figure 7A) exhibit negative anomalies in Nb and Ta and differ from positive anomalies in Initial Rift Tholeiite (IRT, [25]), thus preventing a relationship with a rifting environment (Figure 11).

A rifting setting was mentioned for the "rosary of ditches" of the "Central African" discontinuity in Southern Chad, and would have occurred during rift development after diachronic opening of the South Atlantic during the Early Cretaceous [48, 49]. Negative Nb, Ta and Ti anomalies in Mongo dolerites (Figure 7A) are interpreted as the imprints of older subduction-related magmatism [50] occurring during a previous converging event (Figure 6B and 6C).

From field evidence, dykes would have been emplaced during the last stages of Pan-African orogeny along three different NNE-SSW, NE-SW and ENE-WSW directions which may suggest that they form different swarms [32]. The only geodynamic setting is the "metacratonisation" process which has affected the ancient continental crust of the north-eastern part of Africa [9, 51] combining collisional processes, lithospheric delamination, regional extension, and post-collisional dismembering through strike-slip shearing [9].

6 Conclusion

Dyke swarms crosscutting the granitic basement of Mongo within the Guéra Massif have basalt, to trachybasalt to basaltic trachyandesite compositions and share affinities with continental tholeiites. They exhibit variable doleritic textures, containing phenocrysts, microlites and microcrysts of clinopyroxene, amphibole, plagioclase, alkali feldspar and Fe-Ti oxides. They were emplaced along NNE-

SSW, NE-SW and ENE-WSW trending brittle faults at Pan-African times. Geochemically, they underwent differentiation by fractional crystallization. They may have been generated from partial melting of enriched sub-continental mantle during the final stages of metacratonisation of ancient continental crust of the north-eastern part of Africa, prior to the Mesozoic opening of the South Atlantic Ocean.

Acknowledgement: Authors are grateful to Agence Universitaire de la Francophonie, AUF, through the Bureau Afrique Centrale et des Grands Lacs, BACGL for financial support provided by Projet de Soutien aux Équipes de Recherche, n° 51110SU201. B. Bonin helped us to improve the manuscript. B. Chako Tchamabé and another anonymous reviewer are thanked for useful remarks.

References

[1] Kusnir, I., Moutaye, H.A. (1997) Ressources minérales du Tchad: une revue. Journal of African Earth Sciences, 24, 549-562.

[2] El Makhrouf, A.A. (1988) Tectonic interpretation of Jabal Eghei area and its regional application to Tibesti orogenic belt, south central Libya (S.P.L.A.J.). Journal of African Earth Sciences, 7, 945-967.

[3] Liégeois, J.P. (1992) Rapport sur les mesures des isotopes du Sr en vue de détermination d'âges de roches magmatiques du Sud du Tchad (régions de Baibokoum et de Léré-Figuil). Musée Royal Afrique Centrale, Tervuren, Belgique, 9 p.

[4] Penaye, J., Kroner, A., Toteu, S.F., Van Schmus, W.R., Doumnang, J.C. (2006) Evolution of the Mayo Kebbi region as revealed by zircon dating: An early (ca. 740 Ma) Pan-African magmatic arc in southwestern Chad. Journal of African Earth Sciences, 44, 530-542.

[5] Pouclet, A., Vidal, M., Doumnang, J.C., Vicat, J.P., Tchameni, R. (2006) Neoproterozoic crustal evolution in Southern Chad: Pan-African ocean basin closing, arc accretion and late- to post-orogenic granitic intrusion. Journal of African Earth Sciences, 44, 543-560.

[6] Isseini, M., 2011. Croissance et différenciation crustales au Néoprotérozoïque. Exemple du domaine panafricain du Mayo Kebbi au Sud-Ouest du Tchad. Université Henri Poincaré, Nancy, France, Ph.D. Thesis, 339 p.

[7] Isseini, M., André-Mayer, A.S., Vanderhaeghe, O., Barbey, P., Deloule, E. (2012) A-type granites from the Pan-African orogenic belt in south-western Chad constrained using geochemistry, Sr-Nd isotopes and U-Pb geochronology. Lithos, 153, 39-52.

[8] Isseini, M., Hamit, A., Abderamane, M. (2013) The tectonic and geologic framework of the Mongo area, a segment of the Pan-African Guera Massif in Central Chad: evidences from field observations and remote sensing. Revue Scientifique du Tchad, 1, 3, 4-12.

[9] Abdelsalam, M.G., Liégeois, J.P., Stern, R.J. (2002) Review The Saharan Metacraton. Journal of African Earth Sciences, 34, 119–136.

[10] Frey, F.A., Green, D.H., Roy, S.D. (1978) Integrated models of basalt petrogenesis: a study of quartz tholeiites to olivine melilitites from South Eastern Australia utilizing geochemical and experimental petrological data. Journal of Petrology, 19, 463-513.

[11] Wilkinson, J.F.G., Le Maitre, R.W. (1987) Upper mantle amphiboles and micas and TiO_2, K_2O, and P_2O_5 abundances and 100 Mg/(Mg + Fe2+) ratios of common basalts and andesites: Implications for modal mantle metasomatism and undepleted mantle compositions. Journal of Petrology, 28, 1, 37-73.

[12] Vicat, J.P., Ngounouno, I., Pouclet, A. (2001) Existence de dykes doléritiques anciens à composition de tholéiites continentales au sein de la province alcaline de la ligne du Cameroun. Implication sur le contexte géodynamique. Comptes Rendus de l'Académie des Sciences, Paris, 332, 243-249.

[13] Ngounouno, I., Déruelle, B., Guiraud, R., Vicat, J.P. (2001) Magmatismes tholéiitique et alcalin des demi-grabens crétacés de Mayo Oulo-Léré et de Babouri-Figuil (Nord du Cameroun-Sud du Tchad) en domaine d'extension continentale. Comptes Rendus de l'Académie des Sciences, Paris, IIA, 333, 4, 201-207.

[14] Vicat, J.P., Pouclet, A., Nkoumbou, C., Mouangué, A.S. (1997) Le volcanisme fissural néoprotérozoïque des séries du Dja inférieur, de Yokadouma (Cameroun) et de Nola (RCA) : Signification géotectonique. Comptes Rendus de l'Académie des Sciences, Paris, 325, 9, 671-677.

[15] Crawford, A.J., Stevens, B.P.J., Fanning, M. (1997) Geochemistry and tectonic setting of some Neoproterozoic and Early Cambrian volcanics in western New South Wales. Australian Journal of Earth Sciences, 44, 831-852.

[16] Plank, T., Langmuir, C.H. (1998) The chemical composition of subducting sediment and its consequences for the crust and mantle. Chemical Geology, 145, 3-4, 325-394.

[17] Cabanis, B., Thiéblemont, D. (1988) La discrimination des tholéiites continentales et des basaltes arrière-arc. Proposition d'un nouveau diagramme Th-Tbx3-Tax2. Bulletin de la Société Géologique de France, 8, IV, 6, 927-935.

[18] McDonough, W.F., Sun, S.S. (1995) The composition of the Earth. Chemical Geology, 120, 223-253.

[19] Plank, T. (2005) Constraints from Thorium/Lanthanum on Sediment Recycling at Subduction Zones and the Evolution of the Continents. Journal of Petrology, 46, 921-944.

[20] Cabanis, B., Lécolle, M. (1989) Le diagramme La/10-Y/15-Nb/8: un outil pour la discrimination des séries volcaniques et la mise en évidence des processus de mélange et/ou de contamination crustale. Comptes Rendus de l'Académie des Sciences, Paris, 309, 2023-2029.

[21] Toteu, S.F., Penaye, J., Poudjom Djomani, Y.H. (2004) Geodynamic evolution of the Pan-African belt in central Africa with special reference to Cameroon. Canadian Journal of Earth Science, 41, 1, 73-85.

[22] Miyashiro, A. (1978) Nature of alkalic volcanic rock series. Contributions to Mineralogy and Petrology, 66, 91-104.

[23] Nkouandou, O.F., Fagny Mefire, A., Iancu, G.O., Bardintzeff, J.M. (2015) Petrology and geochemistry of doleritic dyke of Likok (Cameroon, Central Africa). Carpathian Journal of Earth and Environmental Sciences, 10, 1, 121-132.

[24] Ekwueme, B.N. (1994) Basaltic magmatism related to the early stages of rifting along the Benue Trough: the Obudu dolerites of south-east Nigeria. Geological Journal, 29, 269-276.

[25] Holm, P.E. (1985) The geochemical fingerprints of different tectonomagmatic environments using hygromagmatophile ele-

ment abundances of tholeiitic basalts and basaltic andesites. Chemical Geology, 51, 303-323.

[26] Rudnick, R.L., Fountain, D.M. (1995) Nature and composition of the continental crust: a lower crustal perspective. Reviews of Geophysics, 33, 3, 267-309.

[27] Green, T.H., Edgar, A.D., Beasley, P., Kiss, E., Ware, N.G. (1974) Upper mantle source for some hawaiites, mugearites and benmoreites. Contribution to Mineralogy and Petrology, 48, 33-43.

[28] Campbell, I.H. (1985) The difference between oceanic and continental tholeiites: a fluid dynamic explanation. Contributions to Mineralogy and Petrology, 91, 37-43.

[29] Green, T. (1995) Significance of Nb and Ta as an indicator of geochemical processes in the crust-mantle systeme. Chemical geology, 120, 347-359.

[30] Barth, M.G., McDonough, W.F., Rudnick, R.L. (2000) Tracking the budget of Nb and Ta in the continental crust. Chemical Geology, 165, 197–213.

[31] Dupuy, C., Dostal, J. (1984) Trace element geochemistry of some continental tholeiites. Earth and Planetary Science Letters, 67, 61-69.

[32] Ernst, R.E., Head, J.W., Parfitt, E., Grosfils, E., Wilson, L. (1995) Giant radiating dyke swarms on Earth and Venus. Earth-Science Reviews, 39, 1-58.

[33] Ionov, D.A., Hofmann, A.W. (1995) Nb-Ta-rich mantle amphiboles and micas: Implications for subduction-related metasomatic trace element fractionations. Earth and Planetary Science Letters, 131, 341-356.

[34] Allègre, C.J., Dupré, B., Richard, P., Rousseau, D., Brooks, C. (1982) Subcontinental versus suboceanic mantle, II. Nd-Sr-Pb isotopic comparison of continental tholeiites with mid-ocean ridge tholeiites, and the structure of the continental lithosphere. Earth and Planetary Science Letters, 57, 25-34.

[35] Sun, S.S., McDonough, W.F. (1989) Chemical and isotopic systematics of oceanic basalts: implications for mantle composition and processes. In: Saunders, A.D., Norry, M.J., Ed., Magmatism in the Ocean Basins. Geological Society, London, Special Publication, 42, 313-345.

[36] Halliday, A.N., Lee, D.C., Tommasini, S., Davies, G.R., Paslick, C.R., Fitton, J.G., James, D.E. (1995) Incompatible trace elements in OIB and MORB and source enrichment in the sub-oceanic mantle. Earth and Planetary Science Letters, 133, 379-395.

[37] Weaver, B.L., Tarney, J. (1981) The Scourie dyke suite: Petrogenesis and geochemical nature of the Proterozoic sub-continental mantle. Contributions to Mineralogy and Petrology, 78, 175-178.

[38] Wayne, T.J. (1987) Lithophile elements in Huronian low-Ti continental tholeiites from Canada, and evolution of the Precambrian mantle. Earth and Planetary Science Letters 85, 4, 401-415.

[39] Hofmann, A.W., Jochum, K.P., Seufert, M., White, W.M. (1986) Nb and Pb in oceanic basalts: new constraints on mantle evolution. Earth and Planetary Science Letters, 90, 297-314.

[40] Hofmann, A.W. (1988) Chemical differentiation of the Earth: the relationship between mantle, continental crust and oceanic crust. Earth and Planetary Science Letters, 90, 297-314.

[41] Dupuy, C., Liotard, J.M., Dostal, J. (1992) Zr/Hf fractionation in intraplate basaltic rocks: carbonate metasomatism in the mantle source. Geochimica et Cosmochimica Acta, 56, 2417-2423.

[42] Prytulak, J., Elliott, T. (2007) TiO_2 enrichment in ocean island basalts. Earth and Planetary Science Letters, 263, 388-403.

[43] Hawkesworth, C.J., Kempton, P.D., Rogers, N.W., Ellam, R.M., Van Calsteren, P.W. (1990) Continental mantle lithosphere and shallow level enrichment processes in the Earth's mantle. Earth and Planetary Science Letters, 96, 256-268.

[44] Jakeš, P., Gill, J. (1970) Rare Earth elements and the Island arc tholeiite series. Earth and Planetary Science Letters, 9, 17-28.

[45] Wood, D.A. (1980) The application of Th-Hf-Ta diagram to problems of tectonomagmatic classification and to establishing the nature of crustal contamination of basaltic lavas of the British tertiary volcanic province. Earth and Planetary Science Letters, 50, 11-30.

[46] Taylor, B., Martinez, F. (2003) Back-arc basin basalt systematics. Earth and Planetary Science Letters, 210, 481-497.

[47] Tian, L., Castillo, P.R., Hawkins, David, R.J., Hilton, W., Hanan, B.B., Pietruszka, A.J. (2008) Major and trace element and Sr–Nd isotope signatures of lavas from the Central Lau Basin: Implications for the nature and influence of subduction components in the back-arc mantle. Journal of Volcanology and Geothermal Research, 178, 657-670.

[48] Reyre, D. (1984) Remarques sur l'origine et l'évolution des bassins sédimentaires africains de la côte atlantique. Bulletin de la Société Géologique de France, 7, XXVI, 6, 1041-1059.

[49] Guiraud, R., Maurin, J.C. (1991) Le rifting en Afrique au Crétacé inférieur: synthèse structurale, mise en évidence de deux étapes dans la genèse des bassins, relations avec les ouvertures océaniques péri-africaines. Bulletin de la Société Géologique de France, 162, 5, 811-823.

[50] Kelemen, P.B., Shimizu, N., Dunn, T. (1993) Relative depletion of niobium in some arc magmas and the continental crust: partitioning of K, Nb, La and Ce during melt/rock reation in the upper mantle. Earth and Planetary Science Letters, 120, 111-134.

[51] Liégeois, J.P., Abdelsalam, M.G., Ennih, N., Ouabadi, A. (2013) Metacraton: Nature, genesis and behavior. Gondwana Research, 23, 220-237.

[52] Le Maitre, R.W. (Ed.) (2002) Igneous Rocks, A Classification and Glossary of Terms. (Recommendations of the IUGS Subcommission on the Systematics of Igneous Rocks). Cambridge University Press, Cambridge, 252 p.

[53] Saunders, A.D., Storey, M., Kent, R.W., Norry, M.J. (1992) Consequences of plume–lithosphere interactions. In: Storey, B.C., Alabaster, T., Pankhurst, R.J. Ed., Magmatism and the Causes of Continental Break-up. Geological Society, London, Special Publication, 68, 41-60.

[54] Gill, R. (2010) Igneous rocks and processes: A practical guide. Wiley-Blackwell, 440 p.

[55] Maluski, H., Coulon, C., Popoff, M., Baudin, P. (1995) $^{40}Ar/^{39}Ar$ chronology, petrology and geodynamic setting of Mesosoic to early Cenozoic magmatism from the Benue Trough, Nigeria. Journal of the Geological Society, London, 152, 311-326.

[56] Pearce, J.A., Bender, J.F., De Long, S.E., Kidd, W.S.F., Low, P.J., Guner, Y., Saroglu, F., Yilmaz, Y., Moorbath, S., Mitchell, J.G. (1990) Genesis of collision volcanism in Eastern Anatolia, Turkey. Journal of Volcanology and Geothermal Research, 44, 1, 189-229.

[57] Nkouandou, O.F., Bardintzeff, J.M., Dourwe Dogsaye, P., Fagny Mefire, A. (2016) Geochemistry and petrogenesis of mafic doleritic dykes at Mbaoussi (Adamawa plateau, Cameroon, Central Africa). Journal of Geography, Environment and Earth Science International, 8, 1, 1-18, 28198.